

High Frequency Single Crystal Ultrasonic Transducers for High Resolution Ophthalmic Imaging Applications

Tianfu Zhang^{1,2}, Ruimin Chen², Zhiqiang Zhang², K. Kirk Shung², Xingui Tang^{1#} and Qifa Zhou^{2,3*}

¹School of Physics & Optoelectric Engineering, Guangdong University of Technology, Guangzhou Higher Education Mega Center, Guangzhou 510006, People's Republic of China

²NIH Resource Center for Medical Ultrasonic Transducer Technology and Department of Biomedical Engineering, University of Southern California, Los Angeles, CA 90089, USA

³Roski Eye Institute, Department of Ophthalmology, University of Southern California, Los Angeles, CA 90033, USA

*Corresponding Author: Qifa Zhou, University of Southern California, Los Angeles, CA 90033, USA.

#Corresponding Author: Xingui Tang, Guangdong University of Technology, Guangzhou 510006, People's Republic of China.

Received: October 09, 2017; Published: October 13, 2017

Abstract

As one of the most important and well established tools, ultrasound imaging provides noninvasive valuable diagnostic information, especially in the form of cross-sectional images of soft tissues. In this work, we report the design, fabrication, and characterization of press-focused LiNbO₃ transducer. The performance of these transducers is in good agreement with the simulation results. Large bandwidth (92%) and high center frequency (75 MHz) are obtained. The lateral resolution and axial resolution are 110 μm and 13.09 μm respectively. The high resolution imaging capability of the transducer is demonstrated by scanning a pig eyes. The fine structures of pig eye are discernible with these ultrahigh frequency transducers.

Keywords: High frequency; Ultrasound; Ophthalmic imaging; High resolution

Abbreviations: Pb (Zr, Ti)O₃: PZT; Pb (Mg_{1/3}Nb_{2/3})O₃-PbTiO₃: PMN-PT; LiNbO₃: LNO; (K, Na)NbO₃: KNN; (Bi, Na)TiO₃: BNT; BaTiO₃: BT; Bandwidth: BW; Maximum output voltage: V_{pp}; Ultrasound Biomicroscopy: UBM; the resonance frequency: f_r; Anti-resonance frequency: f_a; the center frequency: f_c

Volume 1 Issue 4 October 2017

© All Copy Rights Reserved by Qifa Zhou., et al.

Introduction

Ultrasound has been used in many fields, including chemistry, nuclear physics, biology, medicine, underwater communication technology, materials testing and so on [1-5]. As one of the most important and well established tools, ultrasound imaging provides noninvasive valuable diagnostic information, especially in the form of cross-sectional images of soft issues [6]. Ultrasonic transducers are widely

Citation: Qifa Zhou., et al. "High Frequency Single Crystal Ultrasonic Transducers for High Resolution Ophthalmic Imaging Applications". *Ophthalmology and Vision Science* 1.4 (2017): 135-141.

used in medical detection, nondestructive evaluation, sonar and etc. [7,8], and they are typically classified into single element and array transducers, depending on the number of active elements [9,10]. In terms of frequency, ultrasonic transducers can also be categorized into low-frequency, high-frequency (> 20 MHz), based on their center frequencies. Conventional center frequencies of ultrasonic transducers typically work at frequencies below 50 MHz, which provide tens of microns to millimeter spatial resolution [11-15]. In many applications, such as: eye, blood vessels, etc., high-frequency ultrasonic transducers with better resolution are needed, it is essential to use higher frequency ultrasonic transducers with broader bandwidth and higher resolution. The need for improving image resolution has prompted intensive studies in developing high-frequency imaging systems. High frequency ultrasound is currently used for various imaging applications in ophthalmology.

At present, the choice of piezoelectric material for medical transducer are mostly $Pb(Zr,Ti)O_3$ (PZT) based ceramics and relaxor materials $Pb(Mg_{1/3}Nb_{2/3})O_3-PbTiO_3$ (PMN-PT) single crystals due to their superior piezoelectric properties [16-19]. But due to the environment problem, an available alternative of lead free piezoelectric materials have been studied, such as: $LiNbO_3$ (LNO) single crystal, $(K,Na)NbO_3$ (KNN) based ceramics, PVDF, $(Bi,Na)TiO_3$ (BNT) based ceramics, and $BaTiO_3$ (BT) based ceramics, these materials have been investigated and exhibit comparable performance to that of the lead-based material mentioned above [14, 20-22]. Among these lead free materials, the single crystal LNO has some excellent material properties for its use as actuator material. Table 1 shows the properties of LNO single crystal compared with other piezoelectric materials. The mechanical quality factor according to manufacturer's data is in the order of 100,000 which is a factor 50-100 higher than the available hard PZT. Also, the dielectric losses are significant smaller. Further, the high Curie temperature of LNO (about 1210 °C) is an interesting property. It enables the possibility to design actuators for a high temperature environment.

Material	kt	d_{33} (pC/N)	$\tan\delta$	ϵT_{33}	V (m/s)	ρ (kg/m ³)	T _c (°C)	Z (MRayl)
LNO	0.57	38.8	0.001	40	7360	4688	1210	34.1
BZT-BCT [23]	0.41	597	0.02	2817	5133	5200	93	26.7
BSZT [24]	0.45	300	0.025	1346	5040	-	-	-
KNN [25]	0.28	154	0.029	664	5690	-	420	25.9
PVDF [1]	0.12-0.15	-33	-	5-13	2200	1780	100	3.9
PZT-5A [16]	0.49	374	0.02	85.5	3694	7750	-	33.7
PMN-PT [16]	0.67	1780	0.0036	797	4608	8000	-	36.8
PZT-5H [26, 27]	0.51	600	0.018	1470	4580	7500	200	30

Table 1: Properties of LNO single crystal with other piezoelectric materials.

V: Longitudinal wave velocity, Z: Acoustic impedance, ϵT_{33} : Permittivity, kt: Electromechanical coupling coefficient, d_{33} : Piezoelectric constant, $\tan\delta$: Dielectric loss, ρ : Mass density.

In this work, we report the design, fabrication, and characterization of press-focused $LiNbO_3$ transducer. Large bandwidth (92% at -6dB) and high center frequency (75 MHz) are obtained from pulse-echo response. Simulation and experimentally measured electrical impedance magnitude show highly accordance. The high resolution imaging capability of the transducer is demonstrated by scanning a pig eyes. The fine structures of pig eye are discernible with these ultrahigh frequency transducers.

Experimental Procedure

In this work, 36°Y cut Lithium Niobate single crystal was selected due to its good electromechanical coupling, low dielectric permittivity, high longitudinal wave velocity and high Curie temperature. A Krimholtz, Leedom, and Mattaei (KLM) model-based simulation software PiezoCAD (Sonic Concepts, Woodinville, WA) was used to design the structure of LNO transducer based on the parameters

in Table 1. Specific design parameters of the transducers, including the aperture size and proper thickness of acoustic stacks were optimized through KLM 14 model-based simulation software PiezoCAD. The design parameters of LNO transducer are listed in Table 2.

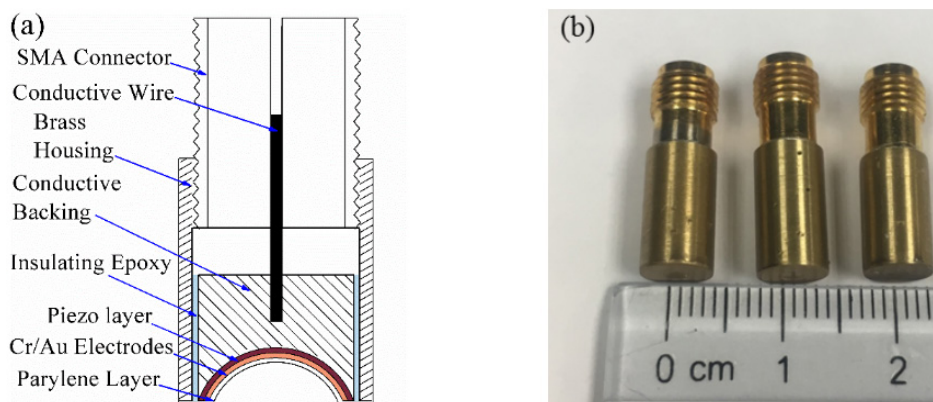


Figure 1: Designed cross section (a) and photograph (b) of LNO transducers.

Due to the relative high frequency, one matching layer was made. Firstly, Cr/Au (50/100 nm) electrode were sputtered on one side of LNO single crystal, and LNO element was lapped to the thickness of about 29.5 μm, this lapping process was carried out with extreme care and in a patient manner. After the deposition of Au/Cr as the electrode on the other side of the ceramic sample, the backing layer E-solder 3022 was then cast on this side as the backing material, which was lapped to 1 mm. The stack was then diced into small posts with aperture of 2.5 mm × 2.5 mm using a dicing saw (Tcar 864-1, Thermocarbon, Casselberry, FL). After pressing focus (6 mm), a lead wire was connected to the backing layer with an additional amount of conductive epoxy, and then a subminiature version A (SMA) connector was fixed to the transducer. A layer of Cr/Au (50 nm/100 nm) was sputtered across the element and the housing to form the ground plane connection. Finally, a thin layer of parylene was vapor-deposited on the front face of the transducer, which served as an acoustic matching layer and a protection layer. Figure 1 showed the schematic fabrication flow of designed transducer structure (a) and prepared transducers (b).

Layer	Piezo Layer	Matching Layer	Backing Layer
Material	LiNiO ₃ Single Crystal	Parylene	E-Solder 3022
Thickness	29.5 μm	7.5 μm	1 mm
Acoustic impedance	34.1 MRayls	2.6 MRayls	5.9 MRayls

Table 2: Parameters of the components of LNO transducer.

Results and Discussions

The electrical impedance characteristics of the transducer were measured by an electric impedance analyzer (HP 4294A, Agilent Technologies, Santa Clara, CA). Figure 2 shows the simulation (a) and experimentally measured (b) electrical impedance magnitude and phase of LNO transducer as a function of frequencies in air. From simulation results: the resonance frequency (f_r) and anti-resonance frequency (f_a) of the transducer are about 107 MHz and 128 MHz, respectively. For experimentally measured impedance results, it is observed that the resonance frequency (f_r) and anti-resonance frequency (f_a) of the transducer are about 100 MHz and 120 MHz, respectively. Clearly, experimentally measured impedance shows highly agreement with simulation results.

In addition, a conspicuous peak in the phase curve is observed both in simulation and measured results. At around 110 MHz, a peak appeared in measured phase curves, it matches well with simulation results (peak in the phase curve: 118 MHz). At the frequency of measured phase curve peak, the electrical impedance is about 40 Ω, which was very close to 50 Ω required by electrical impedance matching of system. The negative phase (-12°) shows the capacitive nature of the device.

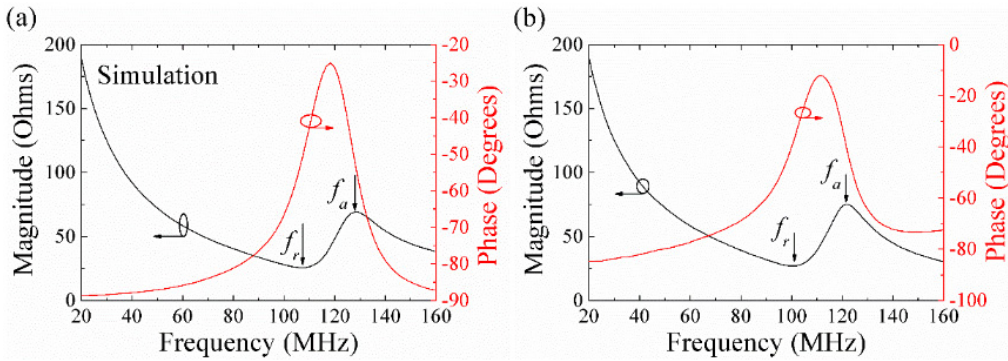


Figure 2: (a) Simulation and (b) measured electrical impedance magnitude and phase of LNO transducers.

According to the IEEE standard, the thickness mode electromechanical coupling coefficient (k_t) should be given by:

$$k_t = \sqrt{\frac{\pi f_r}{2 f_a} \tan\left(\frac{\pi f_a - f_r}{2 f_a}\right)}$$

where f_r and f_a are the resonant frequency (frequency of minimum impedance) and anti-resonant frequency (frequency of maximum impedance) respectively [2,18,28]. According to above equation, k_t is calculated to be 0.606, which is in agreement with the k_t of LiNiO_3 reported elsewhere.

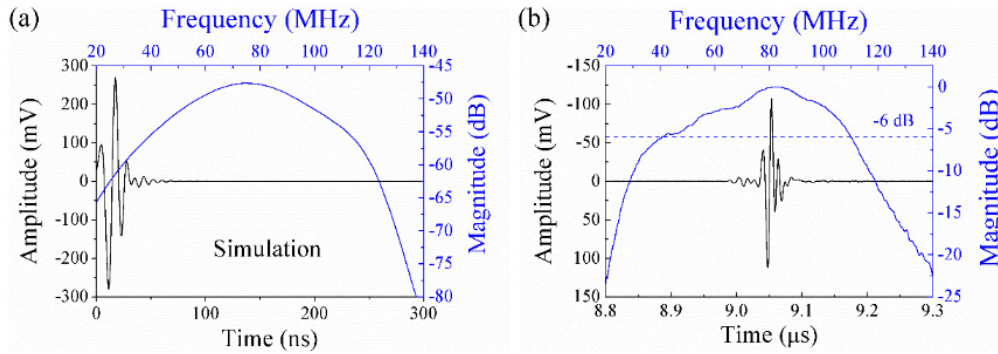


Figure 3: (a) Simulation and (b) measured pulse-echo waveform and frequency spectrum of LNO transducers.

The time domain pulse-echo response and normalized frequency spectrum of the modified LNO transducer are shown in Figure 3. The transducer is connected to a JSR Ultrasonics DPR 500 (Imaginant, Pittsford, NY) pulser/receiver and excited by an electrical impulse at 200 Hz repetition rate and 50 Ω damping. The energy involved is 2.3 μJ and no gain was applied in excitation or reception. An X-cut quartz plate is placed at the focal point as a target. The center frequency (f_c) and -6 dB fractional bandwidth (BW) are determined by [23]: $f_c = (f_l + f_u)/2$, $\text{BW} = (f_u - f_l)/f_c \times 100\%$, where f_l and f_u are defined as lower and upper -6 dB frequencies, respectively, at which the magnitude of the amplitude in the spectrum is 50% (-6 dB) of the maximum. According to above equations, the measured central frequency of the transducer is about 75 MHz, which shows lower values comparing with the electrical impedance, the deviation should be closely to attenuation. The fractional bandwidth at -6 dB is approximately 92%, which is much higher than previous reports of high

frequency transducers [18,29]. The focal length calculated from pulse-echo response is about 6.5 mm, which shows good agreement with our press focus. And the maximum output voltage (V_{pp}) of the unamplified pulse echo is about 0.22 V using the pulser/receiver with 2.3 μ J energy setup.

The imaging capability of the LNO transducer is studied by scanning wire phantom and porcine eyeball. In this study, a customized ultrasound biomicroscopy (UBM) system is used. The transducer is driven by a motor controller card (DMC-1802; Galil Motion Control Inc., Mountain View, CA), which also generat a signal to trigger data acquisition. The Panametrics 5900PR pulser/receiver is used to excite the transducer. A logarithmic compression algorithm is used to improve gray scale visualization of the image. Each 2-D frame of image data is obtained by scanning the transducer and collecting pulse-echo lines at 5 μ m spacing. Firstly, a 20- μ m-diameter tungsten wire phantom (California Fine Wire Company, Grover Beach, CA) is used for this measurement. The three phantom wires are arranged diagonally with equal distance in the axial (1.8 mm) and lateral (0.65 mm) directions. The pulse-echo image is acquired as the transducer scanned across the wire phantom placed in degassed water.

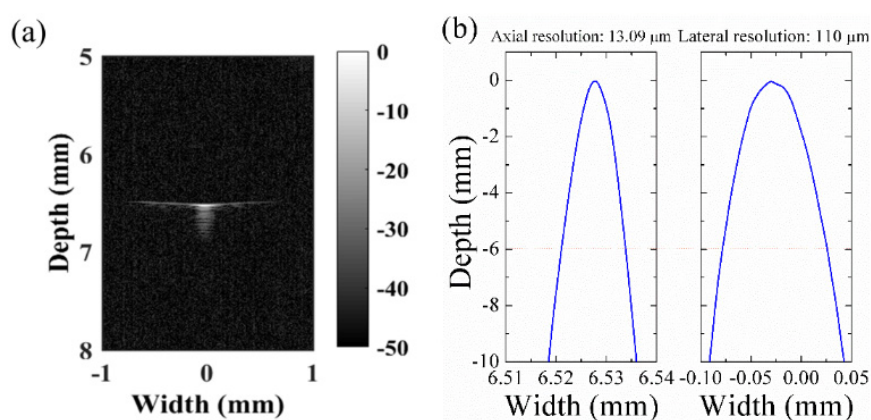


Figure 4: (a) Wire phantom images of LNO transducers with dynamic range of 50 dB, (b) axial resolution, and lateral resolution of LNO transducers.

Ultrasonic transducers with frequency higher than 30 MHz yield improve spatial resolution at the expense of a reduced depth of penetration. The resolution of ultrasound image is determined by the pulse bandwidth (axial resolution, R_{axial}) and the beam width (lateral resolution, lateral). Simple expressions for the ideal lateral and axial resolution of a focused transducer within the focal zone are given by [1,11]: Axial resolution (-6dB): $R_{axial} = \lambda/2BW = C/2f_c BW$; Lateral resolution: $R_{lateral} = \lambda F\#$, where C is the speed of sound in the medium, f_c is the center frequency of the transducer, BW is the bandwidth of the transducer, $F\#$ is the f-number (the ratio of focal distance to aperture dimension) and λ the wavelength. Thus, for a fixed number of cycles per pulse, an increase in frequency would result in a reduction in wavelength and pulse duration (increase in BW) [1].

Figure 4(a) shows the images generated using the LNO transducer with a dynamic range of 50 dB. Axial and lateral beam profiles are shown in Figure 4(b). At about 6.5 mm, the -6 dB axial and lateral resolutions for the needle transducer were 13.09 μ m and 110 μ m, respectively. The measured axial resolution is in approximate agreement with the theoretically predicted axial resolution of 10.5 μ m.

In addition, a porcine eyeball is imaged using this transducer. The porcine eyeball specimen as well as the structure diagram of its eye is presented in Figure 5 the anterior portion image of the porcine eye is conducted with a dynamic range of 90 dB. As shown in Figure 5, the anatomy of porcine eye including the cornea, iris, sclera, lens and iris can be clearly visualized. This image displays a good single-to-noise ratio. These promising results demonstrate that the transducer has very good performance.

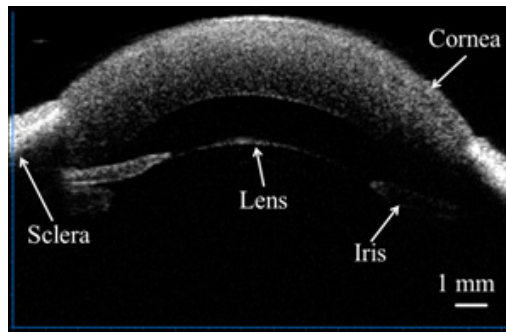


Figure 5: Images of the anterior portion of a porcine eye.

Conclusions

In this work, we report the design, fabrication, and characterization of press-focused LiNbO₃ transducer. The performance of these transducers are in good agreement with the simulation in terms of center frequency, bandwidth. And wide bandwidth (92%) and high center frequency (75 MHz) are obtained. wire imaging of the transducers shows a lateral resolution of 110 μm and an axial resolution of 13.09 μm. The high resolution imaging capability of the transducer is demonstrated by scanning a pig eyes. The fine structures of pig eye are discernible with these ultrahigh frequency transducers.

Acknowledgements

This work was supported by the National Institute of Health under grant R01-EB10090 and P41-EB002182, the National Natural Science Foundation of China (Grant No. 11574057), the Science and Technology Program of Guangdong Province of China (Grant No. 2016A010104018).

References

1. Zhou Q., *et al.* "Piezoelectric films for high frequency ultrasonic transducers in biomedical applications". *Progress in Materials Science* 56.2 (2011): 139-174.
2. Wang K., *et al.* "An imaging model incorporating ultrasonic transducer properties for three-dimensional optoacoustic tomography". *IEEE Transactions on Medical Imaging* 30.2 (2011): 203-214.
3. Silverman R H. "High-resolution ultrasound imaging of the eye - a review". *Clinical & Experimental Ophthalmology* 37.1 (2009): 54-67.
4. Kolkman R G., *et al.* "Real-time in vivo photoacoustic and ultrasound imaging". *Journal of biomedical optics* 13.5 (2008): 050510.
5. Taghaddos E., *et al.* "Lead-free piezoelectric materials and ultrasonic transducers for medical imaging". *Journal of Advanced Dielectrics* 5.2 (2015): 1530002.
6. Hsu H-S., *et al.* "Focused high frequency needle transducer for ultrasonic imaging and trapping". *Applied Physics Letters* 101.2 (2012): 024105.
7. Aristizábal O., *et al.* "44-MHz LiNbO₃/sub 3/transducers for UBM-guided Doppler ultrasound". *IEEE Trans Ultrason Ferroelectr Freq Control* 50.6 (2003): 623-630.
8. Spedicato L., *et al.* "Clustering and PCA for reconstructing two perpendicular planes using ultrasonic sensors". *International Journal of Advanced Robotic Systems* 10.4 (2013): 210.
9. Cannata J M., *et al.* "Design of efficient, broadband single-element (20-80 MHz) ultrasonic transducers for medical imaging applications". *IEEE transactions on ultrasonics, ferroelectrics, and frequency control* 50.11 (2003): 1548-1557.
10. Ketterling J A., *et al.* "Design and fabrication of a 40-MHz annular array transducer". *IEEE transactions on ultrasonics, ferroelectrics, and frequency control* 52.4 (2005): 672-681.
11. Ma T., *et al.* "Systematic study of high-frequency ultrasonic transducer design for laser-scanning photoacoustic ophthalmoscopy". *Journal of Biomedical Optics* 19.1 (2014): 16015.

12. Amini M H., *et al.* "A New High-Temperature Ultrasonic Transducer for Continuous Inspection". *IEEE Trans Ultrason Ferroelectr Freq Control* 63.3 (2016): 448-455.
13. Wang D., *et al.* "Fabrication and characterization of annular-array, high-frequency, ultrasonic transducers based on PZT thick film". *Sensors and Actuators A: Physical* 216 (2014): 207-213.
14. Brodal E., *et al.* "Performance of an Ultrasonic Imaging System Based on a 45-MHz Linear PVDF Transducer Array: A Numerical Study". *Advances in Acoustics and Vibration* 2011 (2011): 1-15.
15. Wong C M., *et al.* "Development of a 20-MHz wide-bandwidth PMN-PT single crystal phased-array ultrasound transducer". *Ultrasonics* 73 (2017): 181-186.
16. Kim K B., *et al.* "Fabrication and comparison of PMN-PT single crystal, PZT and PZT-based 1-3 composite ultrasonic transducers for NDE applications". *Ultrasonics* 50.8 (2010): 790-797.
17. Chen X., *et al.* "Simulation and fabrication of 0–3 composite PZT films for ultrahigh frequency (100–300 MHz) ultrasonic transducers". *Journal of Applied Physics* 119.9 (2016): 094103.
18. Yue Q., *et al.* "Fabrication of a PMN-PT single crystal-based transcranial Doppler transducer and the power regulation of its detection system". *Sensors* 14.12 (2014): 24462-24471.
19. Zhang S., *et al.* "Characterization of Mn-modified Pb(Mg(13)Nb(23))O(3)-PbZrO(3)-PbTiO(3) single crystals for high power broad bandwidth transducers". *Applied Physics Letters* 93.12 (2008): 122908.
20. Bah M., *et al.* "Ultrasonic transducers based on undoped lead-free (K0.5Na0.5)NbO3 ceramics". *Ultrasonics* 63 (2015): 23-30.
21. Chen J., *et al.* "Bandwidth improvement of LiNbO3 ultrasonic transducers by half-concaved inversion layer approach". *Review of Scientific Instruments* 83.11 (2012): 114903.
22. Chan H L W., *et al.* "Bismuth sodium titanate based lead-free ultrasonic transducer for microelectronics wirebonding applications". *Ceramics International* 34.4 (2008): 773-777.
23. Yan X., *et al.* "Lead-free intravascular ultrasound transducer using BZT-50BCT ceramics". *IEEE Trans Ultrason Ferroelectr Freq Control* 60.6 (2013): 1272-1276.
24. Lee S T., *et al.* "High-frequency ultrasonic transducer based on lead-free BSZT piezoceramics". *Ultrasonics* 51.7 (2011): 811-814.
25. Hagh N M., *et al.* "Lead-free piezoelectric ceramic transducer in the donor-doped K 1/2 Na 1/2 NbO 3 solid solution system". *IEEE Trans Ultrason Ferroelectr Freq Control* 55.1 (2008): 214-224.
26. Liu C., *et al.* "High-frequency (50–100MHz) medical ultrasound transducer arrays produced by micromachining bulk PZT materials". *Ultrasonics Symposium* (2008): 690-693.
27. Liu D., *et al.* "Broadband and high sensitive time-of-flight diffraction ultrasonic transducers based on PMNT/epoxy 1-3 piezoelectric composite". *Sensors* 15.3 (2015): 6807-6817.
28. Fei C., *et al.* "Ultrahigh Frequency (100 MHz-300 MHz) Ultrasonic Transducers for Optical Resolution Medical Imaging". *Scientific Reports* 6 (2016): 28360.
29. Chen Y., *et al.* "High performance relaxor-based ferroelectric single crystals for ultrasonic transducer applications". *Sensors* 14.8 (2014): 13730-13758.

Submit your next manuscript to Scientia Ricerca Open Access and benefit from:

- Prompt and fair double blinded peer review from experts
- Fast and efficient online submission
- Timely updates about your manuscript status
- Sharing Option: Social Networking Enabled
- Open access: articles available free online
- Global attainment for your research

Submit your manuscript at:

<https://scientiaricerca.com/submit-manuscript.php>